Quantum transport through pairs of edge states of opposite chirality at electric and magnetic boundaries

Puja Mondal,[1] Alain Nogaret,[2] and Sankalpa Ghosh[1]
[1]*Department of Physics, Indian Institute of Technology Delhi, New Delhi-110016, India*
[2]*Department of Physics, University of Bath, Bath BA2 7AY, United Kingdom*

(Received 26 March 2018; revised manuscript received 21 July 2018; published 11 September 2018)

We theoretically investigate electrical transport in a two-dimensional electron system hosting bulk and edge current carrying states. Spatially varying magnetic and electric confinement creates pairs of current carrying lines that drift in the same or opposite directions depending on whether confinement is applied by a magnetic split gate or a magnetic strip gate. We study the electronic structure through calculations of the local density of states and conductivity of the channel as a function of the chirality and wave-function overlap of these states. We demonstrate a shift of the conductivity peaks to high or low magnetic field depending on the chirality of pairs of edge states and the effect of chirality on backscattering amplitude associated with collisional processes.

DOI: 10.1103/PhysRevB.98.125303

I. INTRODUCTION

In a spatially modulated transverse magnetic field, electrons acquire guiding center drift velocity due to the magnetic field gradient even in the absence of an electric field [1–6]. This strongly modifies the quantum transport of two-dimensional electron gas (2DEG) due to the formation of chiral current carrying states in the otherwise insulating bulk of a quantum Hall system [7]. However, compared to the prototype quantum Hall system in a uniform magnetic field [8,9], the magnetically modulated quantum Hall system has received much less attention. There have been interesting experimental developments through the observation of an asymmetric magnetoconductance peak in a quantum wire [10], a resistance resonance effect due to magnetic edge states [11,12], magnetoresistance oscillations as a result of the commensurability effect [13–16], giant magnetoresistance [17–21], and transport assisted by snake orbits [22–24]. The properties of graphene in a nonuniform magnetic field have also attracted attention [25–36]. In a recent work, a magnetoresistance anomaly has been observed in a quantum Hall system due to the controlled interference between magnetic edge states and conventional electrostatic edge states [37].

In this paper, we theoretically investigate two representative hybrid ferromagnetic-semiconductor structures in which magnetic and electrostatic edge states propagate parallel or antiparallel to one another. These edge states propagate in the same direction under a magnetic split gate whereas they propagate in opposite directions under a bar magnet. We emphasize on the differences of the electronic band structure of the two devices through local density of states (LDOS) and density of states (DOS) calculations. Our calculations are based on energy levels and wave functions calculated in realistic magnetic potentials. Further, we calculate the bulk and edge transport properties understanding the different contributions of co-propagating and counterpropagating states. Our findings demonstrate hybrid structures as a unique laboratory for studying the interactions of low-dimensional phases in the bulk and the edges of quantum-Hall-like systems.

Using an electrostatic gate to gradually deplete the sample edges, we are able to control the overlap between the wave functions of electrostatic and magnetic edge states. We find that when edge states are far apart the quantum transport is quasiadiabatic (full suppression of interedge channel scattering [38]). The amplitude of magnetoresistance oscillations is independent of the magnetic potential. As edge state overlap increases, the edge states that drift in opposite directions give magnetoresistance oscillations that rapidly increase in amplitude. In contrast, no change is observed when edge states drift in the same direction. This leads us to conclude that backscattering between counterpropagating edge states enhances the collisional conductivity of the strip gate device whereas elastic scattering between edge states drifting forward shows little change in conductivity in the magnetic split gate. Hence we predict that transport measurements can evidence the chiral/nonchiral nature of one-dimensional localized edge states.

Accordingly, the rest of the paper is arranged as follows. In Sec. II, we model the electronic structure of the magnetic split and strip gate and the methodology to solve the Hamiltonian. The local density of states and density of states was calculated to compare the electronic structure of both devices. We discuss the effects of lateral confinement on the LDOS and DOS. In Sec. III, we compute the conductivity tensor within the quantum Boltzmann equation and model the effect of edge state chirality on the disorder conductivity. We describe the resistivity in both magnetic split and strip gate for the decreasing values of lateral confinement.

II. ELECTRONIC STRUCTURE OF THE SPLIT AND STRIP GATES

A. Model Hamiltonian

We consider a 2DEG modulated by a perpendicular magnetic field in two different ways as depicted in Fig. 1. By using a magnetic split gate or a magnetic strip gate, two magnetic modulations can be produced which have inverted profiles.

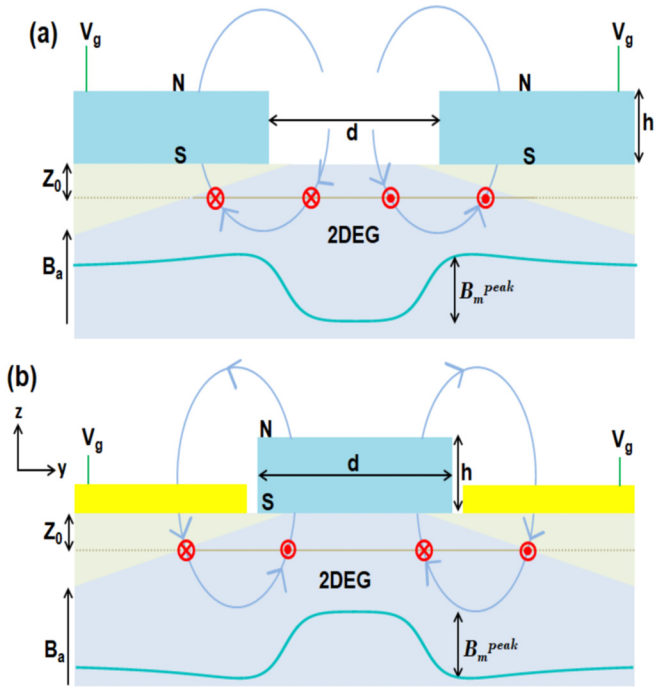

FIG. 1. Schematic diagram of the quantum Hall devices: (a) magnetic split gate and (b) magnetic strip gate. The stray magnetic field originating from the magnetic gate modulates the 2DEG. Green and yellow slabs represent the ferromagnetic and normal metal gate. The approximate position and drift direction of edge states is shown by the arrows (red color). The electrical width of the 2D channel W_e is controlled by the gate voltage V_g. The depletion region underneath the gate is shown by the light brown line. B_m^{peak} is the peak value of the modulated magnetic field.

A bias voltage is applied to the split magnetic gate in Fig. 1(a) and to the normal metal gate sandwiching the ferromagnetic gate in Fig. 1(b) to deplete the 2DEG underneath. Through the combination of electrostatic and magnetic potentials, both systems confine electrostatic and magnetic edge states (red arrows). In the magnetic split gate (a), electrostatic and magnetic edge states always drift in the same direction. In the magnetic strip gate (b), the inverted magnetic field gradient causes the magnetic edge states to drift in the opposite direction to the electrostatic edge states. Therefore in this system it is important to study both edge versus bulk conduction and conduction via chiral versus nonchiral pairs of edge states. We write the total magnetic field as

$$B(y) = B_m^{\uparrow\uparrow/\downarrow\uparrow}(y) + B_a, \tag{1}$$

where $B_m^{\uparrow\uparrow/\downarrow\uparrow}$ and B_a are the modulated and uniform magnetic field. $\uparrow\uparrow$ / $\downarrow\uparrow$ refers to the co-propagating (split gate) or counterpropagating edge states (strip gate) as plotted in Fig. 2:

$$\begin{aligned} B_m^{\uparrow\uparrow}(y) &= -\frac{\mu_0 M_s}{2\pi}[f_0^+(y) - f_0^-(y) - f_h^+(y) + f_h^-(y)], \\ B_m^{\downarrow\uparrow}(y) &= \frac{\mu_0 M_s}{2\pi}[f_0^+(y) - f_0^-(y) - f_h^+(y) + f_h^-(y)], \end{aligned} \tag{2}$$

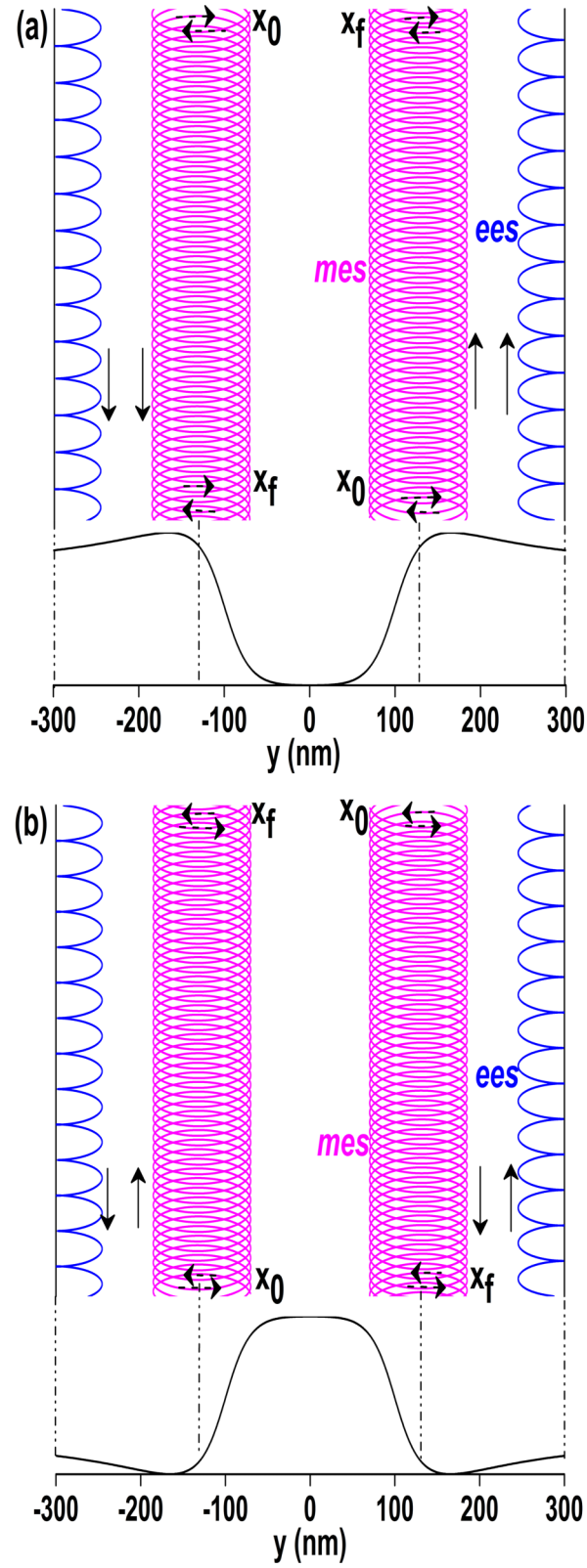

FIG. 2. Semiclassical picture of edge states in the magnetic split (a) and strip (b) gate for $\mu_0 M_s = 2.90$ T and $B_a = 2$ T. *mes* and *ees* are the classical orbits of magnetic and electrostatic edge states. Modulation magnetic field is shown by the black curve. *mes* and *ees* are drifting in the same direction (co-propagating edge states) in the magnetic split gate while they drift in opposite direction (counterpropagating edge states) in the strip gate.

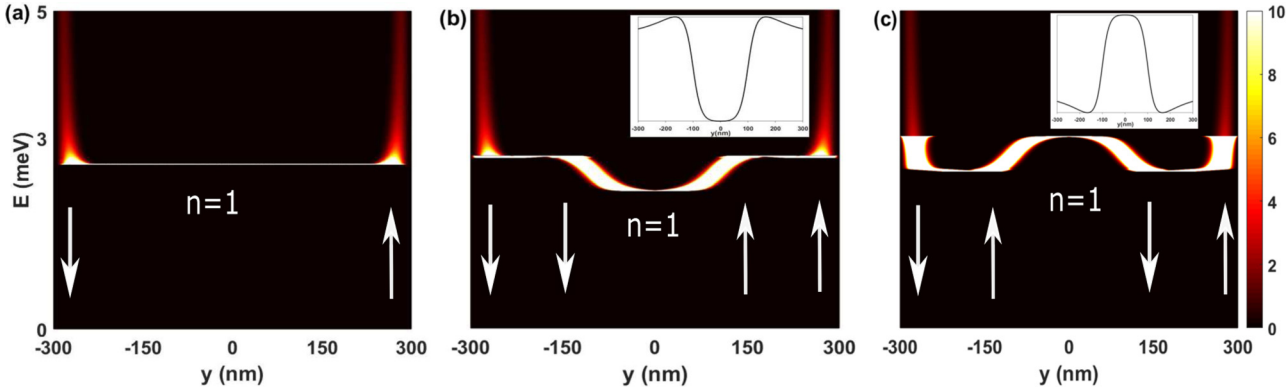

FIG. 3. LDOS of the lowest energy energy level at $B_a = 3$T for (a) zero magnetic modulation, (b) magnetic split, and (c) magnetic strip gate. LDOS replicates the magnetic field profile for nonzero modulation, whereas it does not show any variation for zero modulation. The arrow indicates the drifting direction of edge states.

where $f^{\pm}_{z=\{0,h\}}(y) = \text{atan}(\frac{y\pm d/2}{z_0+z})$. We define h as the thickness of the magnet, d is the distance between the two magnets (split gate) or the width of the magnet (strip gate), z_0 is the depth of the 2DEG, and $\mu_0 M_s$ is the saturation magnetization. As a representative case, we choose some experimentally realizable values as $d = 200$ nm, $h = 80$ nm, $z_0 = 30$ nm, and $\mu_0 M_s = 2.90$ T (Dy) [37]. The peak value of the modulated magnetic field [green curve in Figs. 1(a) and 1(b)] is estimated from Eq. (2) and found to be $B_m^{\text{peak}} = 0.65$ T for both devices as can be obtained from dysprosium magnets.

The distance between lines of zero magnetic field where the magnetic modulation changes sign is defined as W_m. From the modulated magnetic field profile (Fig. 2), W_m can be calculated as 274 nm. This system has a finite magnetic field gradient centered at $y \approx \pm W_m/2$. The gate voltage induces an electrostatic potential to the system resulting in the depletion of 2DEG. We model the electrostatic potential as a square well potential of width W_e:

$$V(y) = \begin{cases} V_0 = 700 \text{ meV}, & \text{for } |y| \geq W_e \\ 0, & \text{for} |y| \leq W_e \end{cases}. \tag{3}$$

We choose few representative values of W_e from the recent experiment as 600, 400, and 250 nm [37].

The Hamiltonian of a two-dimensional electron gas (2DEG) in such magnetic modulation and electrostatic confinement is

$$H = \frac{1}{2m^*}\left[p_y^2 + (p_x + eA_x(y))^2 + V(y)\right], \tag{4}$$

where $A_x(y)$ is the vector potential corresponding to the magnetic field given in Eq. (1) and m^* is the effective mass of electron. We consider a Landau gauge [$\mathbf{A} = (A_x(y), 0, 0)$] and we numerically solve Eq. (4) (by relaxation method [39]) to obtain the energy levels and the wave function. The wave-vector dependent effective potential is of the form $V_{\text{eff}}(\bar{y}, \bar{k}_x) = [\bar{k}_x + \bar{A}(\bar{y})]^2$, which has a reflection symmetry when changing the sign of k_x/y giving an energy spectrum that is symmetric about the center of the Brillouin zone. We define $\bar{k}_x = k_x l_b$, $\bar{y} = y/l_b$, where $l_b = \sqrt{\hbar/eB_0} = 25.66$ nm for a uniform magnetic field of strength $B_0 = 1$ T. The length and momentum are expressed in units of l_b and l_b^{-1}. The unit of energy is $E_0 = \frac{\hbar^2}{2m^* l_b^2} = 0.8622$ meV.

The interesting physics in the two devices (magnetic split and strip gate) resides in the existence of edge states (magnetic edge states) at the center of the wire drifting in the magnetic gradient with a guiding center following the $y = W_m/2$ line. These states propagate in the forward or backward direction depending on the sign of the magnetic field gradient. Thus, depending on their velocity direction, magnetic edge states either co-propagate or counter-propagate with the electrostatic edge states. For that, we calculate the drift velocity of semiclassical orbits at the Fermi level in the magnetic field gradient as [40]

$$v_d = \frac{\omega_0 r_g^2}{2} \frac{\nabla \boldsymbol{B}_m \times \boldsymbol{B}_m}{(B_m)^2},$$

where B_m is the modulated magnetic field generated by the magnetic gate, ω_0 and r_g are the gyration angular frequency and radius. The magnetic field gradient (∇B_m) at y $= W_m/2$ is positive for the magnetic split gate [Fig. 2(a)], which makes the magnetic edge states drift in the positive x direction causing a parallel motion of the magnetic edge states with respect to the electrostatic edge states, whereas in the magnetic strip gate a negative magnetic field gradient at y $= W_m/2$ results in an antiparallel motion of the magnetic edge states with respect to the electrostatic edge states [Fig. 2(b)].

B. Electronic band structure

The formation of edge states at the center of the quantum Hall system is demonstrated through the calculated local density of states (LDOS) [41,42]. LDOS is obtained from the energy and the eigenfunction of the 2DEG and is defined as

$$\rho(E, y) = \sum_{\alpha} \delta(E - E_\alpha)|\psi_\alpha(y)|^2, \tag{5}$$

where $\alpha = \{n, k_x\}$ is a quantum state.

The LDOS of $n = 0$ level is shown in Fig. 3 for $B_a = 3$T. LDOS does not show variation when the magnetic modulation is absent [Fig. 3(a)]. The energy levels are degenerate with respect to k_x (or the location of the center of oscillator) for

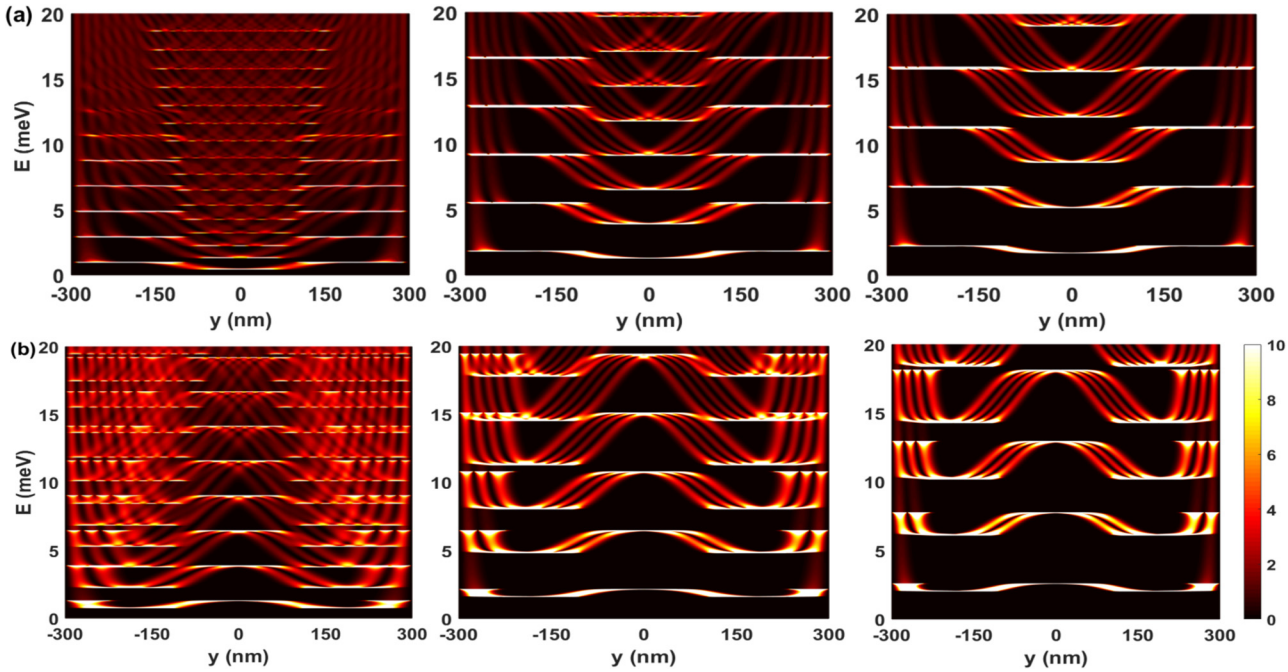

FIG. 4. LDOS for a fixed channel width $W_e = 600$ nm at different values of $B_a = 1$, 2, and 2.5 T for the split (a) and strip (b) gates. At $B_a = 2.5$ T, the magnetic minibands are separated from each other in the strip gate while they overlap in the split gate.

zero magnetic modulation. The modulated magnetic field lifts the Landau level degeneracy near the center of the channel. This leads to the formation of states of lower energy at the center in the split gate [Fig. 3(b)] and of higher energy in the strip gate [Fig. 3(c)].

At high magnetic field ($\omega_a >> \omega^{\uparrow\uparrow/\downarrow\downarrow}$), the quantized energy levels of the magnetic edge states (about the center of the channel) can be described using an approximate energy relation $\bar{E}_n(\bar{k}_x) = (n + 1/2)\hbar(\omega_m^{\uparrow\uparrow/\downarrow\downarrow}(\bar{k}_x) + \omega_a)$, where $\omega_m^{\uparrow\uparrow/\downarrow\downarrow}(\bar{k}_x) = \frac{eB_m^{\uparrow\uparrow/\downarrow\downarrow}(\bar{k}_x)}{m^*}$ and $\omega_a = \frac{eB_a}{m^*}$. The group velocity $(dE_{n,\bar{k}_x}/d\bar{k}_x)$ at y $= W_m/2$ is positive for magnetic split gate while it is negative for magnetic strip gate. The chirality of magnetic edge states reverses in the magnetic strip gate. As a result, the LDOS is a convenient tool to visualize the modification of energy levels by the combined effects of the inhomogeneous magnetic field and the electrostatic potential, which is experimentally accessible to scanning tunneling microscopy [43].

Figure 4 shows the LDOS computed at different values of the applied magnetic field $B_a = 1$, 2, and 2.5 T in the split and strip gate channels of constant width $W_e = 600$ nm. In this figure, the formation of a subset of interference pattern in the magnetic minibands in the central region appears due to the interference between magnetic edge states in different Landau levels. At finite magnetic field gradient, multiple branches are visible at each energy level which overlaps with the consecutive energy level branches at lower magnetic field ($B_a = 1$ T in Fig. 4). The number of branches at each energy level becomes clearly visible as B_a increases ($B_a = 2$ and 2.5 T in Fig. 4). Since the LDOS is directly proportional to the probability density of the electrons [Eq. (5)], the number of branches in the dispersion curves demonstrates the number of nodes in the wave function of the edge states. The finite gradient of the energy spectrum therefore gets split into $n + 1$ branches for the nth Landau level where the magnetic field has finite gradient. However, the splitting vanishes where the magnetic field gradient is approximately zero and the dispersion is flat at $y = 0$ and 200 nm for the profiles considered in this paper. Also, the energy separation between the adjacent Landau bands varies over the region and becomes large when the magnetic field gradient is steeper.

Magnetic minibands overlap in energy at low magnetic field. However, above a critical magnetic field, energy gaps open between magnetic minibands. It appears from the band calculations that minigaps occur at different B_a in the split gate and strip gate. As for example at $B_a = 2.5$ T, a gap occurs between the magnetic minibands at the Fermi energy ($E_F = 16.9$ meV) in the strip gate [Fig. 4(b)], while magnetic minibands still overlap with each other at Fermi energy at $B_a = 2.5$ T in the split gate [Fig. 4(a)]. Such a gap opens in the magnetic minibands when the energy gap between consecutive energy levels at the center of the Hall channel ($y = 0$) becomes larger than the magnetic bandwidth (demonstrated in Fig. 5). In the presence of a homogeneous magnetic field only, the energy gap between consecutive energy levels is constant and of the form $\hbar\omega_a = \frac{\hbar e}{m^*}B_a$. However, in the presence of magnetic modulation, the energy gap between consecutive energy levels (E_g) at the center of the modulation (as shown in Fig. 5) in the split gate becomes

$$E_g^{\uparrow\uparrow} = (E_{n+1} - E_n)_{y=0} = \frac{\hbar e}{m^*}\left(B_a - B_m^{\text{peak}}\right), \tag{6}$$

while in the strip gate

$$E_g^{\uparrow\downarrow} = (E_{n+1} - E_n)_{y=0} = \frac{\hbar e}{m^*}\left(B_a + B_m^{\text{peak}}\right). \tag{7}$$

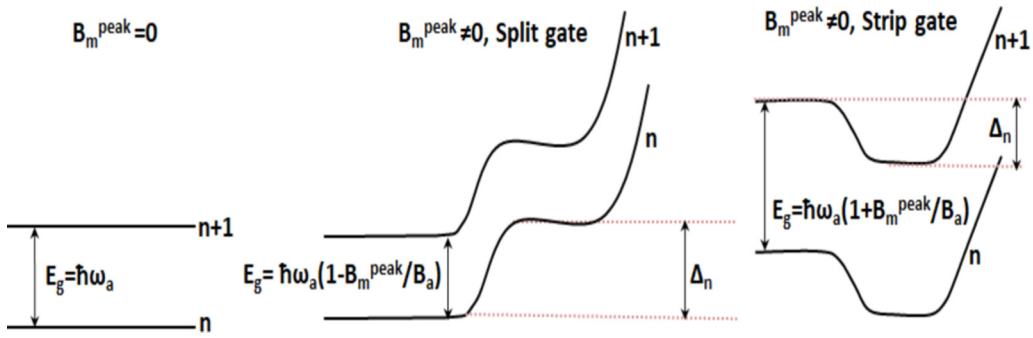

FIG. 5. Schematic of gap opening phenomenon in the magnetic minibands in the split and strip gate. Since the modulated magnetic field increases the energy gap between consecutive energy levels in the strip gate, the minimum magnetic field required to open a gap in the magnetic minibands is smaller than the split gate.

The reason of which is that the negative magnetic modulation at the center in the split gate decreases the energy gap between consecutive energy levels by $\frac{\hbar e}{m^*}B_m^{\text{peak}}$, whereas positive magnetic modulation in the strip gate increases the energy gap by $\frac{\hbar e}{m^*}B_m^{\text{peak}}$. The magnetic bandwidth (Δ_n) is of the form

$$\begin{aligned}\Delta_n &= |\max(E_n) - \min(E_n)| \\ &= (n+1/2)\frac{\hbar e B_m^{\text{peak}}}{m^*}. \end{aligned} \tag{8}$$

Thus, when $E_g > \Delta_n$, the magnetic minibands are separated from each other and a gap opens in the magnetic minibands. The minimum magnetic field required to open a gap in the magnetic minibands in the split gate is given as

$$\begin{aligned} E_g^{\uparrow\uparrow} &\approx \Delta_n, \\ B_a^{\uparrow\uparrow} &= (n+3/2)B_m^{\text{peak}}. \end{aligned} \tag{9}$$

So, the magnetic field at which a gap opens is n dependent. The subband n that contributes to electrical conductivity is the one crossing the Fermi level hence satisfying the condition $(n_F + 1/2) = \frac{E_F}{\hbar\omega_a}$. By replacing $(n_F + 1/2) = \frac{E_F}{\hbar\omega_a}$ in Eq. (9), one gets

$$B_a^2 - B_m^{\text{peak}}B_a - B_F B_m^{\text{peak}} = 0, \tag{10}$$

where $B_F = \hbar k_F^2/2e$ and k_F is the Fermi wave vector. The applied magnetic field at which minigaps open in the split gate is of the form

$$B_a^{\uparrow\uparrow} = \frac{B_m^{\text{peak}} + \sqrt{\left(B_m^{\text{peak}}\right)^2 + 4B_F B_m^{\text{peak}}}}{2}. \tag{11}$$

We obtain the corresponding magnetic field for the strip gate by replacing B_m^{peak} with $-B_m^{\text{peak}}$ in Eq. (11). We evaluate $B_a^{\uparrow\uparrow} = 2.8$ T for a split gate and $B_a^{\downarrow\uparrow} = 2.2$ T for the strip gate [Fig. 4(b)] using $B_m^{\text{peak}} = 0.65$ T. The gap opening in the magnetic minibands leads to large amplitude oscillation in the density of states (DOS) and also in the conductivity.

Figure 6 plots the LDOS at a fixed value of $B_a = 3$T for decreasing values of channel width $W_e = 600$ nm, 400 nm, and 250 nm. For wider channel width ($W_e = 600$ nm), the magnetic and electrostatic edge states are separated by $\sim 8\ell_b$ resulting in a small overlap of their wave function. But as electrostatic confinement increases, the overlap of the electronic wave function increases. When $W_e < W_m$, the magnetic edge states are depleted leaving behind only the electrostatic edge states. Thus, as one decreases W_e, the electrostatic edge states cross over the magnetic edge states.

We have plotted the DOS of both devices as a function of applied magnetic field in Fig. 7. The DOS is given as

$$D(E) = D_0\hbar\omega\sum_n\int dk_x\, P_{\text{imp}}\left(E - E_{n,k_x}\right), \tag{12}$$

where $P_{\text{imp}}(E - E_{n,k_x}) = \frac{1}{\Gamma\sqrt{\pi}}\exp\left(-\frac{(E-E_{n,k_x})^2}{\Gamma^2}\right)$ is the Gaussian broadening induced by the impurity with Γ being full width at half maximum. The Gaussian tails of the density of states assume screened random impurities with a Gaussian potential [44,45]. The screening is assumed to be constant. The realization of a narrow channel by a split magnetic gate [37] allows otherwise localized states in Gaussian tails to bridge opposite edges. For this reason and because we consider intermediate magnetic fields where the longitudinal resistance does not vanish in the Landau gaps, the assumption of Gaussian broadening holds. Equation (12) accounts for both modulation and impurity broadening of the energy levels. The small amplitude oscillations at lower B_a correspond to the overlap of magnetic minibands. At high B_a, the small amplitude oscillations also occur besides the high amplitude oscillation for the wider channel of width $W_e = 600$ nm ($*$ symbols in Fig. 7). These oscillations appear due to the existence of magnetic minibands. But as W_e decreases, the depletion of magnetic minibands (as shown in Fig. 6 for $W_e =$ 400 and 250 nm) causes the small amplitude oscillation to die out. Also, the peaks shift to a higher magnetic field [split gate in Fig. 7(a)] or lower magnetic field [strip gate in Fig. 7(b)] as W_e decreases from 600 nm to 400 nm. The shift of the peak position as a function of W_e can be understood from the LDOS plot for various values of W_e, which is shown in Fig. 6. The magnetic minibands are successively depleted as we increase the electrostatic confinement. When W_e decreases from 600 nm to 400 nm, the peak in the DOS shifts from the edge to the band center which is lower in energy [Fig. 6(a)]. Therefore decreasing W_e causes the maxima of DOS to shift lower in energy. To keep the highest occupied band aligned with the Fermi level, a higher magnetic field is required resulting in a shift of the peak position to a higher magnetic field [Fig. 7(a)].

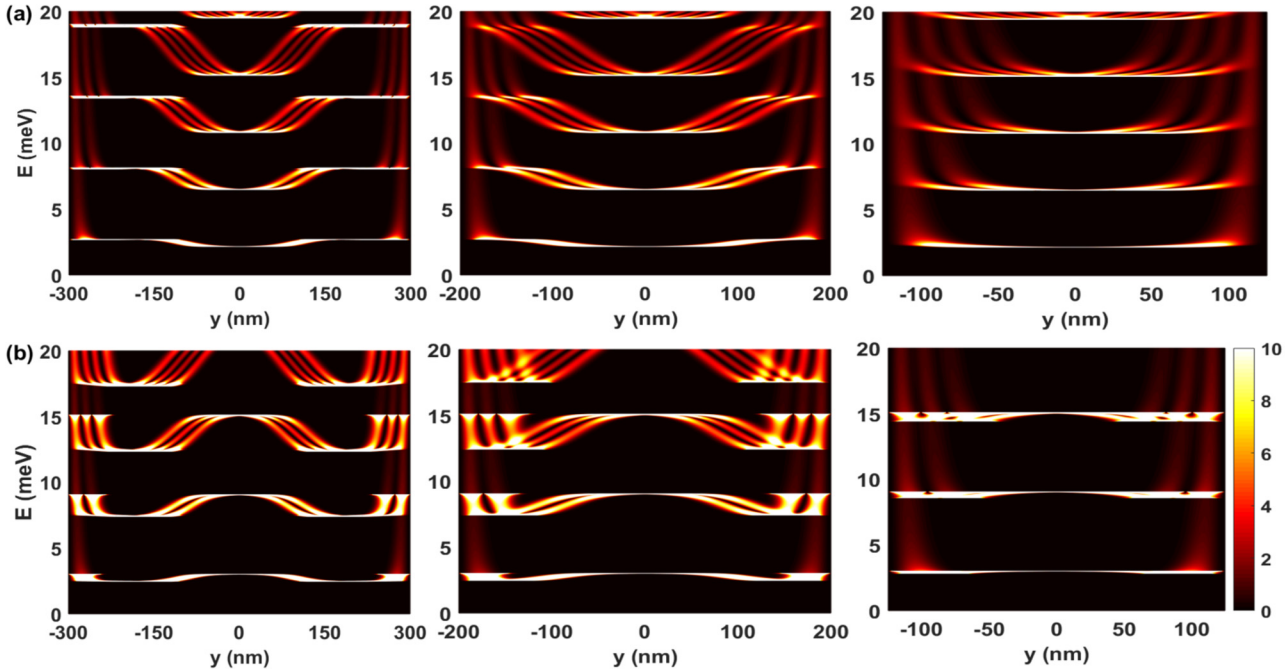

FIG. 6. LDOS for a fixed $B_a = 3$ T at channel widths $W_e = 600$, 400, and 250 nm in the split (a) and strip (b) gate. As channel width decreases, the overlap of magnetic and electrostatic edge states increases resulting in increasing back scattering in the strip gate (b).

As W_e further decreases, peaks shift to a lower magnetic field due to the decreasing value of the Fermi energy.

In contrast, the DOS peaks in the strip gate shift to a lower magnetic field when W_e decreases from 600 to 400 nm. In this case, positive modulation at the center lowers the energy of the magnetic minibands [Fig. 6(b)]. This results in DOS maxima shifting higher in energy. Thus the applied magnetic field has to decrease to keep the central Landau levels aligned with the Fermi level causing LDOS peaks to shift to lower magnetic fields. From $W_e = 400$ to 250 nm, peaks shift to the lower magnetic fields because of the decrease in electron density (or Fermi energy).

III. CONDUCTIVITY TENSOR AND MAGNETORESISTANCE

We calculate the magnetoresistance of the strip and split gate systems to quantify the effects of different electronic structures and the chiral/nonchiral nature of edge state transport. We use linear response theory to determine the current density J as a response to a weak applied electric field E [46]. The linear response theory and the Landauer-Büttiker approach present advantages and drawbacks for the treatment of this problem. The linear response regime was preferred because transport properties could be modelled smoothly through the transition from the diffusive regime ($\omega_a\tau < 1$) to the quantum regime ($\omega_a\tau > 1$) up and until localized states form and zero resistance minima are observed. The latter regime appears well after the onset of resistance oscillations—and Hall plateaux—in the narrow channels we consider. The linear response theory is also useful to account for bulk-edge interactions.

In the presence of a weak field and disorder, the conductivity tensor contains both diagonal and nondiagonal parts, which come from the diagonal/nondiagonal part of the current density operator, which has been calculated in Ref. [47]. The conductivity tensor is

$$\sigma_{\mu,\nu}(\omega) = \sigma^{d}_{\mu,\nu}(\omega) + \sigma^{nd}_{\mu,\nu}(\omega) \text{ with } \mu,\ \nu = x,\ y,\ z, \quad (13)$$

where d and nd are the diagonal and nondiagonal parts of the conductivity tensor. We calculate various contributions to the conductivity tensor in the static limit ($\omega \to 0$). The diagonal components of the conductivity tensor consist of the band conductivity and the scattering/collisional conductivity:

$$\sigma^{d}_{\mu,\nu}(\omega) = \sigma^{\text{band}}_{\mu,\nu}(\omega) + \sigma^{\text{coll}}_{\mu,\nu}(\omega). \quad (14)$$

The band contribution of the conductivity is of the form

$$\sigma^{\text{band}}_{\mu\nu} = \frac{\beta e^2}{A} \sum_{n,k_x} \int dE\ P_{\text{imp}} \times \left(E - E_{n,k_x}\right) f_E(1 - f_E)\tau(E) \upsilon^{n,k_x}_{\mu}\ \upsilon^{n,k_x}_{\nu}, \quad (15)$$

where $\beta = 1/k_B T$, A is the area of the sample, f_E is the Fermi-Dirac distribution function, $\tau(E)$ is the relaxation time, and υ^{n,k_x}_{μ} is the velocity operator given as $\frac{1}{\hbar}\frac{\partial E_{n,k_x}}{\partial k_\mu}$. Electrons are free particles along the x direction, while localized along the y direction, i.e, $\upsilon_y = 0$. Therefore the band conductivity along the y direction is zero, i.e., $\sigma^{\text{band}}_{yy} = 0$, and also $\sigma^{\text{band}}_{xy} = \sigma^{\text{band}}_{yx} = 0$. The band conductivity along the x direction is

$$\sigma^{\text{band}}_{xx} = \frac{e^2}{h}\frac{\tau}{L_y\hbar\sqrt{\pi}\Gamma} \sum_{n} \int dE \left(-\frac{\partial f}{\partial E}\right) \int dk_x \times \exp\left(-\frac{\left(E - E_{n,k_x}\right)^2}{\Gamma^2}\right) \left|\frac{\partial E_{n,k_x}}{\partial k_x}\right|^2. \quad (16)$$

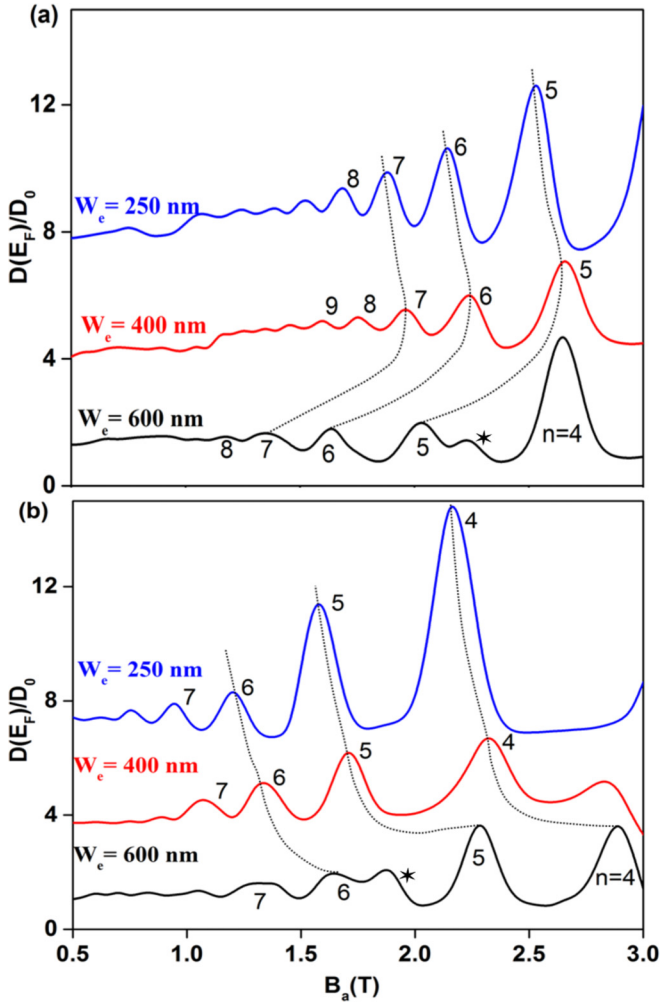

FIG. 7. Density of states at the Fermi energy vs applied magnetic field in the split gate (a). Peaks shift to a higher magnetic field when the electrostatic confinement width decreases from 600 to 400 nm, while peaks shift to a lower magnetic field in the split gate (b). ∗ symbols denote the small amplitude oscillations due to magnetic minibands.

The band conductivity weakly depends on the temperature and its dependence is similar in split and strip gates (depicted in Fig. 3 in Ref. [48]).

Collision conductivity considers the transport through localized states in the presence of impurities. We consider $\sigma_{xx}^{\rm coll} = \sigma_{yy}^{\rm coll}$ due to isotropic impurity scattering. The collisional contribution to the conductivity ($\sigma_{xx}^{\rm coll}$) with broadening is given by [49]

$$\sigma_{xx}^{\rm coll} = \frac{\beta e^2}{A}\sum_{\xi\xi'}\int dE\int dE' P(E-E_\xi)P(E'-E_{\xi'}) \times f(E)[1-f(E')]W_{\xi\xi'}(E,E')\left(\alpha_x^{\xi}-\alpha_x^{\xi'}\right)^2, \quad (17)$$

where $W_{\xi\xi'}$ is the transition rate between $|\xi\rangle$ and $|\xi'\rangle$ and $\alpha_x^{\xi} = \langle nk_x|x|nk_x\rangle$ is the expectation value of position operator and $|\xi\rangle = |n,k_x\rangle$. We consider elastic scattering for which $f(E) = f(E')$. The transition rate is given as

$$W_{\xi\xi'}(E,E') = \frac{2\pi N_I}{A\hbar}\sum_q |U_q|^2|\langle\xi|e^{iq.r}|\xi'\rangle|^2\delta(E-E'). \quad (18)$$

U_q is the Fourier transform of the impurity potential $U(r-R) = \frac{e^2}{4\pi\epsilon\epsilon_0|r-R|}e^{-k_s|r-R|}$; r and R are the position of the electron and impurity, respectively, k_s is the screening wave vector, and N_I is the impurity density. We consider only the dominant term $n = n'$ (intralevel scattering) and next-nearest interlevel scattering term, i.e., $n-n' = \pm 1$, which is sufficient because the scattering rate decreases exponentially with the distance between the centers of oscillator: $k_s = q_s k_F$, $q_s = \frac{2^{3/2}me^2}{\epsilon\hbar^2\sqrt{4\pi n_s}} \to k_s \simeq k_F$, $U_0 = \frac{e^2}{2\epsilon\epsilon_0}$ and $l_b = \sqrt{\hbar/eB}$.

In a relatively dirty 2DEG like the shallow 2DEGs, which we have considered, disorder is greater than the case considered by Fogler *et al.* [50]. If a tail of localized states exists between Landau levels then there would be no edge to edge scattering and the longitudinal resistance would be zero. Experiments show that zero longitudinal resistance minima occur at a magnetic field above the onset of the Landau quantization. This is why the linear response theory is the appropriate theory. At a higher magnetic field (or larger τ), the formation of localized bands, the percolation threshold, and extended states are in a grey theoretical regime between Boltzmann and Landauer-Büttiker. It can be noted that in the magnetic/electric cross-over experiment [37], the wire is in a very narrow channel (100 to 200 nm), making it easier for the localized states in the tail to bridge the two edges, hence, be delocalized—more delocalized than in the typical Hall bar used to investigate the quantum Hall system.

In order to compare the effects of co-propagating states at the edges of the split gate and counterpropagating edge states at the edges of the strip gate, we have plotted the contributions of intraband scattering [Fig. 8(a)] and interband scattering [Fig. 8(b)]. Because disorder induces elastic transitions, conduction takes place through intraband transitions between broadened Landau levels in the bulk and interband transitions between dispersive subbands at the edges. In the bulk, intra-Landau level impurity assisted scattering is phenomenologically accounted for by Gaussian broadening, which corresponds to a finite energy level lifetime. Intraband scattering can not occur at the edges as same n corresponds to different energies, which is not possible for elastic scattering. Similarly, interenergy level transitions cannot occur in the bulk because impurity scattering conserves energy and the only way an $n \to n+1$ transition may conserve energy is at the edge of the sample. Therefore, inter-Landau level transitions are forbidden in the bulk by energy conservation as long as $\omega_a\tau > 1$. The collisional conductivity is isotropic and in the 2D quantum regime measures the amount of backscattering in the longitudinal direction.

The calculation shows that intraedge scattering is largest at low magnetic field where elastic transitions involves small changes in momentum. Interedge scattering decreases as the magnetic field increases and vanishes at high magnetic field [Fig. 8(b)]. In contrast, the amplitude of intraband

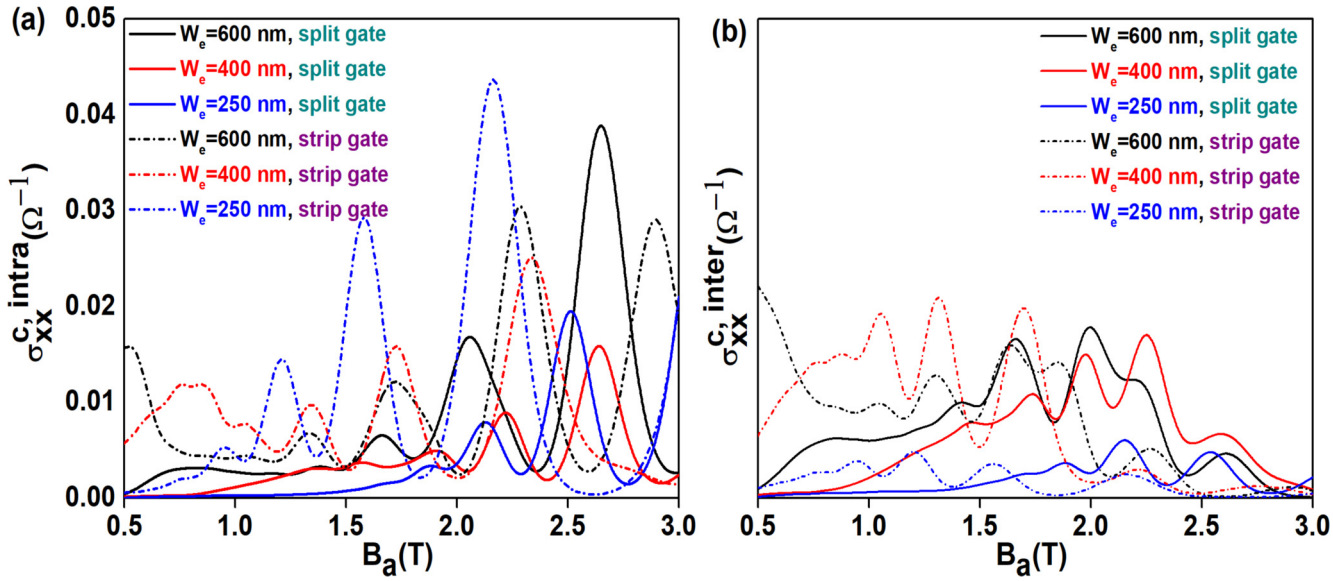

FIG. 8. (a) Intra- and (b) interenergy level collision conductivity as a function of applied magnetic field in the split and strip gate. The intraband scattering measures the transitions in bulk Landau levels where the scattering between magnetic and electrostatic edge is not possible. Whereas the interenergy level scattering occurs between magnetic and electrostatic edge states ($n \rightarrow n+1$), only elastic transition conserving the Landau level index can occur within degenerate Landau levels. We consider $T = 4$ K and $\Gamma = 0.6$ meV.

oscillations continues to increase as B_a increases [Fig. 8(a)]. This is consistent with the corresponding increase in amplitude of Shubnikov de Haas (SdH) oscillations in unmodulated systems at high magnetic field. Figure 8(b) demonstrates that edge backscattering in the quantum regime ($\omega_a\tau > 1$) is greater when edge states propagate in opposite directions (dashed-dotted lines) than in the same direction (solid curves). The criterion for the onset of Landau quantization ($\omega_a\tau > 1$) is actually the energy-time uncertainty principle in which the quantum lifetime is replaced with phenomenological mobility lifetime. Our calculation shows dips in the DOS and the diagonal resistivity ρ_{xx} in between the Landau levels. This shows that the quantum Boltzmann approach provides an appropriate description of the diffusive and quasiadiabatic quantum transport regimes prior to the onset of pure edge conduction [50,51].

The backscattering increases as the overlap of electric and magnetic edges increases from $W_e = 600$ to 400 nm. Thereafter the magnetic edges are depleted and naturally backscattering also decreases (250 nm: dashed dotted blue curve). In contrast, one notes that backscattering is much smaller when edge states are co-propagating in the split gate device [Fig. 8(b), solid curves]. The quantum Boltzmann equation has the advantage of describing both dissipation in the bulk, to model quantum transport experiments, and at the edges through the consideration on intraedge backscattering. The results of Fig. 8, therefore underline the chirality of the pairs of edge states in the split and strip gate systems by

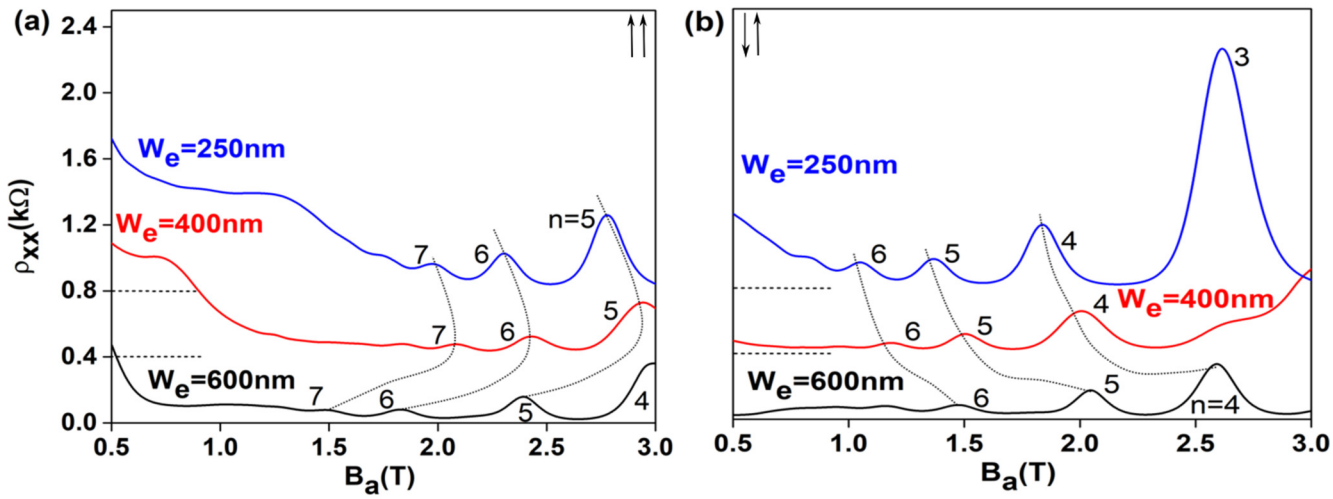

FIG. 9. Magnetoresistance for decreasing channel width in the split (a) and strip (b) gate. Arrow indicates the drifting direction of edge states.

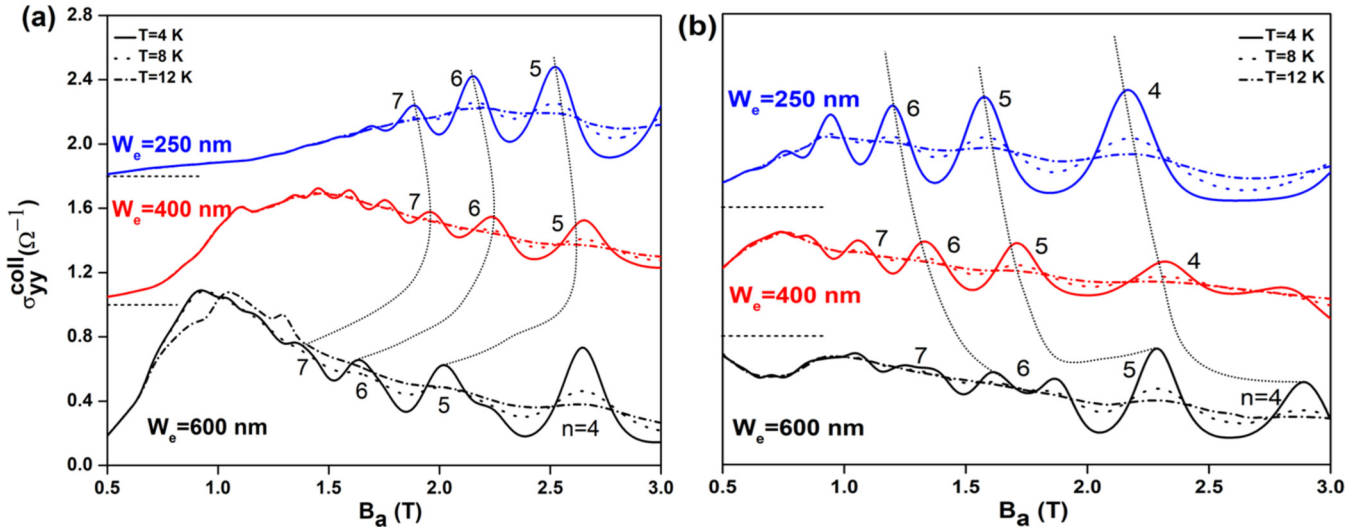

FIG. 10. Collision conductivity as a function of applied magnetic field in the split (a) and strip (b) gates. The amplitude of the oscillations becomes weaker as temperature increases, as expected. Curves are offset vertically for clarity.

showing greater backscattering in the latter, when edge states are counterpropagating.

We have calculated the resistivity including contribution from the band conductivity [Eq. (15)], collision conductivity [Eq. (17)], and the nondiagonal conductivity (Eq. II.2 in Ref. [48]), which we combined in the plot of the longitudinal resistivity shown in Fig. 9. The effect of reducing the channel width is to shift the resistance peaks to a lower magnetic field in the split gate system where the magnetic field at the centre of the Hall channel is lower. In contrast, the resistance peaks move to a higher magnetic field in the strip gate according to the same mechanism as in Fig. 7. The amplitude of the peaks increases when W_e decreases from 600 to 400 nm in the magnetic strip gate because of the increasing overlap of edge states [as $n = 5$ in Fig. 8(b)].

We show the effect of increasing temperature on the conductivity in Fig. 10. The amplitude of oscillations in collisional conductivity decreases as temperature increases. The oscillations are observable when $\hbar\omega_a > k_B T$. The temperature dependence of Shubnikov de Haas oscillations is $\chi/\sinh(\chi)$, $\chi = 2\pi^2 k_B T/\hbar\omega_a$. The chirality effect on the collisional conductivity becomes less significant as the temperature increases.

IV. CONCLUSIONS

In conclusion, we have studied the properties of a 2DEG exposed to two types of modulated magnetic field profile. We have calculated the LDOS, which shows the difference in the electronic structure of the split and strip gate devices. LDOS demonstrates the formation of magnetic edge states near the center of the gate and electrostatic edge states at the boundary. Also, LDOS shows an interference originating from the magnetic miniband subset at the center of the gate. In the split gate, magnetic and electrostatic edge states drift parallel. In contrast, the opposite magnetic field gradient in the strip gate changes the drifting direction of magnetic edge states resulting in antiparallel motion of magnetic and electrostatic edge states.

The calculated collisional conductivity depends on the relative drift directions of magnetic and electrostatic edge states. This dependence is borne by the shape of the wave function in the scattering matrix element. The diffusion and nondiagonal conductivities are independent of drift direction and only contribute to the diffusive conduction regime at low magnetic fields. The resistance peaks at high magnetic fields are dominated by the collisional conductivity and are larger in the case of a strip gate than a split gate device as the channel width decreases. This indicates stronger backscattering in the case of edge states, which propagate in opposite directions (strip gate) in contrast to edge states which propagate in the same direction (split gate). This suggests that the chiral/nonchiral nature of the bulk and edge conducting states might be probed through quantum transport measurements.

ACKNOWLEDGMENTS

This work was supported by a UGC-UKIERI 2013-14/081 thematic award. P. Mondal is supported by UGC fellowship.

[1] J. E. Müller, Phys. Rev. Lett. **68**, 385 (1992).
[2] J. Reijniers and F. M. Peeters, J. Phys.: Condens. Matter **12**, 9771 (2000).
[3] B. Schüler, M. Cerchez, H. Xu, J. Schluck, T. Heinzel, D. Reuter, and A. D. Wieck, Phys. Rev. B **90**, 201111 (2014).
[4] S. Park and H. S. Sim, Phys. Rev. B **77**, 075433 (2008).
[5] H. S. Sim, K. H. Ahn, K. J. Chang, G. Ihm, N. Kim, and S. J. Lee, Phys. Rev. Lett. **80**, 1501 (1998).
[6] P. Hoodbhoy, J. Phys. Condens. Matter **30**, 185303 (2018).
[7] A. Nogaret, J. Phys. Condens. Matter **22**, 253201 (2010).

[8] B. I. Halperin, Phys. Rev. B **25**, 2185 (1982).

[9] A. H. Macdonald, *Quantum Hall Effect: A Perspective* (Kluwer Academic, Dordrecht, 1990).

[10] A. Tarasov, S. Hugger, H. Y. Xu, M. Cerchez, T. Heinzel, I. V. Zozoulenko, U. Gasser-Szerer, D. Reuter, and A. D. Wieck, Phys. Rev. Lett. **104**, 186801 (2010).

[11] A. Nogaret, S. J. Bending, and M. Henini, Phys. Rev. Lett. **84**, 2231 (2000).

[12] A. Nogaret, D. N. Lawton, D. K. Maude, J. C. Portal, and M. Henini, Phys. Rev. B **67**, 165317 (2003).

[13] D. Weiss, K. Klitzing, K. Ploog, and G. Weimann, Europhys. Lett. **8**, 179 (1989).

[14] H. A. Carmona, A. K. Geim, A. Nogaret, P. C. Main, T. J. Foster, M. Henini, S. P. Beaumont, and M. G. Blamire, Phys. Rev. Lett. **74**, 3009 (1995).

[15] P. D. Ye, D. Weiss, R. R. Gerhardts, M. Seeger, K. von Klitzing, K. Eberl, and H. Nickel, Phys. Rev. Lett. **74**, 3013 (1995).

[16] C. Zhang and R. R. Gerhardts, Phys. Rev. B **41**, 12850 (1990).

[17] A. Nogaret, S. Carlton, B. L. Gallagher, P. C. Main, M. Henini, R. Wirtz, R. Newbury, M. A. Howson, and S. P. Beaumont, Phys. Rev. B **55**, R16037 (1997).

[18] N. Overend, A. Nogaret, B. L. Gallagher, P. C. Main, M. Henini, C. H. Marrows, M. A. Howson, and S. P. Beaumont, Appl. Phys. Lett. **72**, 1724 (1998).

[19] G. Papp and F. M. Peeters, J. Phys.: Condens. Matter **16**, 8275 (2004).

[20] X. D. Yang, R. Z. Wang, Y. Guo, W. Yang, D. B. Yu, B. Wang, and H. Yan, Phys. Rev. B **70**, 115303 (2004).

[21] J. W. Yoo, H. W. Jang, V. N. Prigodin, C. Kao, C. B. Eom, and A. J. Epstein, Phys. Rev. B **80**, 205207 (2009).

[22] M. Hara, A. Endo, S. Katsumoto, and Y. Iye, Phys. Rev. B **69**, 153304 (2004).

[23] J. Schluck, S. Fasbender, T. Heinzel, K. Pierz, H. W. Schumacher, D. Kazazis, and U. Gennser, Phys. Rev. B **91**, 195303 (2015).

[24] A. Leuschner, J. Schluck, M. Cerchez, T. Heinzel, K. Pierz, and H. W. Schumacher, Phys. Rev. B **95**, 155440 (2017).

[25] A. De Martino, L. Dell'Anna, and R. Egger, Phys. Rev. Lett. **98**, 066802 (2007).

[26] T. K. Ghosh, A. De Martino, W. Häusler, L. Dell'Anna, and R. Egger, Phys. Rev. B **77**, 081404(R) (2008).

[27] M. Tahir and K. Sabeeh, Phys. Rev. B **77**, 195421 (2008).

[28] M. Ramezani Masir, P. Vasilopoulos, A. Matulis, and F. M. Peeters, Phys. Rev. B **77**, 235443 (2008).

[29] T. Shen, Y. Q. Wu, M. A. Capano, L. P. Rokhinson, L. W. Engel, and P. D. Ye, Appl. Phys. Lett. **93**, 122102 (2008).

[30] M. Ramezani Masir, P. Vasilopoulos, and F. M. Peeters, Appl. Phys. Lett. **93**, 242103 (2008).

[31] L. Dell'Anna and A. De Martino, Phys. Rev. B **80**, 155416 (2009).

[32] Q. H. Huo, R. Z. Wang, and H. Yan, Appl. Phys. Lett. **101**, 152404 (2012).

[33] A. Sandner, T. Preis, C. Schell, P. Giudici, K. Watanabe, T. Taniguchi, D. Weiss, and J. Eroms, Nano Lett. **15**, 8402 (2015).

[34] R. Yagi, R. Sakakibara, R. Ebisuoka, J. Onishi, K. Watanabe, T. Taniguchi, and Y. Iye, Phys. Rev. B **92**, 195406 (2015).

[35] M. R. Thomsen, S. R. Power, A. P. Jauho, and T. G. Pedersen, Phys. Rev. B **94**, 045438 (2016).

[36] N. Agrawal, S. Ghosh, and M. Sharma, Int. J. Mod. Phys. B **27**, 1341003 (2013).

[37] A. Nogaret, P. Mondal, A. Kumar, S. Ghosh, H. Beere, and D. Ritchie, Phys. Rev. B **96**, 081302(R) (2017).

[38] C. W. J. Beenakker and H. van Houten, Solid State Phys. **44**, 1 (1991).

[39] W. H. Press, S. A. Teukolsky, W. T. Vetterling, and B. P. Flannery, *Numerical Recipes in C* (Cambridge University Press, Cambridge, UK, 1994).

[40] J. D. Jackson, *Classical Electrodynamics* (Wiley, New York, 1962), pp. 588-589.

[41] D. L. Miller, K. D. Kubista, G. M. Rutter, M. Ruan, W. A. de Heer, M. Kindermann, P. N. First, and J. A. Stroscio, Nat. Phys. **6**, 811 (2010).

[42] Y. S. Fu, M. Kawamura, K. Igarashi, H. Takagi, T. Hanaguri, and T. Sasagawa, Nat. Phys. **10**, 815 (2014).

[43] R. J. Hamers, Ann. Rev. Phys. Chem. **40**, 531 (1989).

[44] K. Broderix, N. Heldt, and H. Leschke, J. Phys. A: Math. Gen. **24**, L825 (1991).

[45] T. Ando and Y. Murayama, J. Phys. Soc Jpn. **54**, 1519 (1985) and references therein.

[46] R. Abe, *Statistical Mechanics* (University of Tokyo Press, Tokyo, 1975), p. 28.

[47] M. Charbonneau, K. M. Van Vliet, and P. Vasilopoulos, J. Math. Phys. **23**, 318 (1982).

[48] See Supplemental Material at http://link.aps.org/supplemental/10.1103/PhysRevB.98.125303. In Sec. I, we discuss the DOS for decreasing channel width by omitting energy levels broadening. We show band and the nondiagonal conductivity and their dependence on the temperature in Sec. II.

[49] J. Shi, F. M. Peeters, K. W. Edmonds, and B. L. Gallagher, Phys. Rev. B **66**, 035328 (2002).

[50] M. M. Fogler, A. Yu. Dobin, V. I. Perel, and B. I. Shklovskii, Phys. Rev. B **56**, 6823 (1997).

[51] M. Flöser, B. A. Piot, C. L. Campbell, D. K. Maude, M. Henini, R. Airey, Z. R. Wasilewski, S. Florens, and T. Champel, New J. Phys. **15**, 083027 (2013).